CONF-771140--2

AN APPROXIMATE METHOD OF ELASTIC-PLASTIC FRACTURE ANALYSIS FOR NOZZLE CORNER CRACKS*

J. G. Merkle
Oak Ridge National Laboratory
Oak Ridge, Tennessee 37830

ABSTRACT

Two intermediate test vessels with inside nozzle corner cracks have been pressurized to failure at ORNL by the HSST Program. Vessel V-5 leaked without fracturing at 88°C (190°F), and Vessel V-9 failed by fast fracture at 24°C (75°F) as expected. The nozzle corner failure strains were 6.5 and 8.4%, both considerably greater than pretest plane strain estimates. The inside nozzle corner tangential strains were negative, implying transverse contraction along the crack front. Therefore, both vessels were reanalyzed, considering the effects of partial transverse restraint by means of the Irwin β_{Ic} formula. In addition, it was found possible to accurately estimate the nozzle corner pressure-strain curve by either of two semiempirical equations, both of which agree with the elastic and fully plastic behavior of the vessels. Calculations of failure strain and fracture toughness corresponding to the measured final strain and flaw size are made for both vessels, and the results agree well with the measured values.

*Work done at Oak Ridge National Laboratory, operated by Union Carbide Corporation for the Department of Energy; this work funded by U.S. Nuclear Regulatory Commission under Interagency Agreements 40-551-75 and 40-552-75.

INTRODUCTION

The engineering precautions taken to prevent the occurrence of fracture in steel structures are necessary because flaws, which are the basic cause of fracture, sometimes occur despite efforts to the contrary. Nevertheless, most structures that contain flaws do not fail, because the flaws are too small, the loads are not high enough and the material has sufficient fracture toughness to resist unstable crack extension. The development of fracture mechanics methods of analysis has made it possible to quantitatively examine a given structural design and material selection to determine if there are sufficient margins between the specified flaw sizes, material properties and loading conditions, and those that could cause failure. In the case of a welded steel pressure vessel, two types of situations involving flaws need to be considered in a fracture safety analysis. The first is a flaw attempting to propagate out of an embrittled region, wherever one might exist, and the second is the attempted unstable extension of a flaw growing by fatigue in sound material. Precautions against the first type of failure (the nonarrest of a propagating crack) are based on defining the size and shape of a boundary surrounding the embrittled region in sound material and treating this boundary as the size of a crack that must arrest. This is the concept underlying the use of the reference flaw size and the reference (crack arrest) fracture toughness in nuclear pressure vessel design.[1] Precautions against the second type of failure (static initiation of a crack formed and growing by fatigue in sound material) can be based on fracture mechanics analysis methods that use the static initiation fracture toughness. Methods for considering, by analysis, the possible stable growth of cracks under monotonically increasing loads are now being developed,[2-4] but the analysis to be discussed here does not include this phenomenon explicitly. Instead, stable

crack growth will be treated approximately by using a maximum load fracture toughness determined from a test specimen in which some stable crack growth may have occurred before failure. Depending on the method of analysis, the amount of stable crack growth that may occur in the structure before failure may also be estimated, based on previous test data, and added to the original crack size.

STATEMENT OF THE PROBLEM

The particular fracture prevention problem being considered here is that of preventing the unstable extension of a crack formed and growing by fatigue at the inside corner of a nozzle in a pressure vessel. The crack is assumed to lie in the plane containing the axis of both the nozzle and the vessel (the longitudinal plane), because the inside nozzle corner stress concentration factor for pressure loading is known to be a maximum in this plane, and also because cyclic pressure experiments have shown that fatigue cracks form first at this location.[5] The problem is relevant to the fracture safety analysis of nuclear pressure vessels because cracks formed by thermal fatigue have occurred around the inside corners of Boiling Water Reactor (BWR) feedwater nozzles.[6] Previous example calculations have also shown that inside nozzle corner cracks of sufficient initial size can grow appreciably by fatigue[7] thus increasing the importance of determining the accuracy of fracture analysis methods for such flaws. Since local yielding is permitted at nozzle corners by the ASME Code design rules, provided that rules regarding low cycle fatigue prevention can also be satisfied,[8] it is clear that satisfactory margins of safety in terms of load for overload conditions cannot be established for nozzle corner regions containing flaws with only linear elastic fracture mechanics methods of analysis. Therefore there is a need for elastic-plastic fracture analysis methods, simple enough for code application, by which safety margins in terms of load for nozzle corner regions containing flaws

can be established. The intent of this paper is to demonstrate, by means of comparing calculations with experimental data, certain important features of this problem for the case of pressure loading.

EXPERIMENTAL RESULTS AND IMPLICATIONS

Two intermediate test vessels containing nozzles with fatigue sharpened inside nozzle corner cracks, designated Vessels V-5 and V-9, have been tested to failure by the Heavy Section Steel Technology (HSST) Program, which is managed for the U.S. Nuclear Regulatory Commission by the Oak Ridge National Laboratory (ORNL). The design of these vessels is shown in Fig. 1, and a general view of two intermediate test vessels as delivered, one of which contains a nozzle, is shown in Fig. 2. The data pertinent to the analysis of Vessels V-5 and V-9, except for the fracture toughness properties of the nozzle materials, are listed in Table 1. The tests were performed by ORNL, and a detailed report on the testing procedures, analyses, and experimental results is available.[9] The nozzles of both vessels were fabricated from A508 class 2 forging steel. The cylinder of Vessel V-5 was fabricated from A508 class 2 forging steel, and the cylinder of Vessel V-9 was fabricated from A533, grade B, class 1 steel plate. A calculated pressure versus outside surface circumferential strain curve for the vessel cylinders is shown in Fig. 3, for later reference.

Each vessel contained one fatigue sharpened surface crack, approximately 3.05 cm (1.2 in.) deep, in the inside nozzle corner nearest to the vessel head, as indicated in Fig. 1. Each flaw was prepared by first sawing a 20 mm (0.80 in.) deep slot across the nozzle corner; then welding a steel boss over the opening of the slot; next applying cyclic hydraulic pressure to the notch cavity through a hole drilled in the boss until untrasonic measurements made from the outside nozzle corner, in the notch plane, indicated sufficient fatigue flaw

growth; and finally removing the weld boss by flame cutting and grinding. This difficult procedure required cutting, welding and grinding to be done by a man inside the vessel, a process requiring special equipment and safety precautions as described in more detail in Ref. 9. The pretest ultrasonic estimates of crack front depth and shape for Vessels V-5 and V-9 were quite similar.[9] The pretest ultrasonically estimated crack front configuration for Vessel V-9 is shown in Fig. 4. The inflections in the crack front shape are believed to be due to the effects of the weld boss. Their effects on the test results, which are believed to be minor, will be discussed later.

Vessel V-5 was tested first, at 88°C (190°F), and failed by leaking without fast fracturing. Vessel V-9 was tested later, at 24°C (75°F), and failed by fast fracture as expected. Static fracture toughness data for the nozzle material of Vessel V-5 were obtained before the test using precracked Charpy V-notch[9] and a combination of 0.85T and 2.0T compact specimens.[10] Fracture toughness values at maximum load were calculated for each specimen, from its load-displacement diagram, by the equivalent energy procedure.[11] This calculation procedure was justified by the known substantial agreement between J Integral and equivalent energy toughness calculations for the same points on the load-displacement diagrams of notched beams and compact specimens.[12] The Vessel V-5 nozzle precracked Charpy specimens were tested at temperatures between −73°C (−100°F) and 93°C (200°F). The resulting toughness values[9] indicated that, above −18°C (0°F), the static toughness of the Vessel V-5 nozzle material lies within or above the range 159–220 $MNm^{-3/2}$ (145–200 ksi $\sqrt{in.}$). All the Vessel V-5 nozzle compact specimens were tested at 93°C (200°F). The majority of the 0.85T specimens gave toughness values lying in the upper part of the range of the precracked Charpy values, and the two 2.0T specimens tested[9,10] gave toughness values of 245 $MNm^{-3/2}$ (223 ksi $\sqrt{in.}$) and 265 $MNm^{-3/2}$ (241 ksi $\sqrt{in.}$). Considering both the range of data for each specimen size and

the generally observed increase in static upper shelf maximum load toughness values with increasing specimen size, the latter value of 265 $MNm^{-3/2}$ (241 ksi $\sqrt{in.}$) was selected as the toughness value to be used for analyzing the flawed 15.2 cm (6 in.) thick Vessel V-5 nozzle forging.[9]

Static and dynamic fracture toughness data for the nozzle material of Vessel V-9 were obtained before the test, using precracked Charpy V-notch and a combination of 0.85T, 1.5T and 2.0T compact specimens.[9,10] These data are plotted versus temperature in Fig. 5. The vessel test temperature of 24°C (75°F) was selected on the basis of the static precracked Charpy data shown in Fig. 5 and dynamic precracked Charpy data previously obtained[13] for Vessel V-7. The remaining data shown in Fig. 5 were obtained after the vessel test temperature was selected. The objective of the test temperature selection for Vessel V-9 was to choose a temperature, below the dynamic upper shelf temperature, at which the dynamic toughness might be less than the static toughness, in order to produce a fast running fracture as a test result. Preliminary calculations indicated that crack arrest following the onset of rapid fracture would be unlikely, because the increase in crack size would more than offset the decrease in nominal stress near the crack front. The data shown in Fig. 5 indicated that there was no consistent effect of specimen size on the static fracture toughness of the Vessel V-9 nozzle material at 24°C (75°F). This is because (1) the 1.5T specimens gave values near the middle of the static toughness range, (2) both greater and lesser values were obtained from smaller specimens, and (3) the minimum and maximum values were obtained from the 2T specimens. Consequently, it was decided to make static initiation calculations for three toughness values covering the full range of the values measured at 24°C (75°F): 159 $MNm^{-3/2}$ (145 ksi $\sqrt{in.}$), 220 $MNm^{-3/2}$ (200 ksi $\sqrt{in.}$), and 298 $MNm^{-3/2}$ (271 ksi $\sqrt{in.}$). Because the steepest part of the dynamic fracture toughness transition curve occurs at 24°C (75°F) and the range of dynamic values extends from below to above the range of static values, both stable crack growth and "popins" were considered possible.[9]

The result of the test of Vessel V-5 at 88°C (190°F) was a leak without a fracture, which occurred at a pressure of 183 MPa (26,600 psi). The position of the crack front was measured continuously during the test by an ultrasonic sensor located on the outside surface of the nozzle directly opposite the fatigue sharpened crack front. Stable crack growth was first detected at a pressure of 124 MPa (18,000 psi), and above that pressure the crack front continued to advance stably until it penetrated the outer surface near the ultrasonic crystal.[9] The point of leakage was barely visible and there was no visible distortion of the vessel. A closeup view of the point of leakage in Vessel V-5 is shown in Fig. 6. The result of the test of Vessel V-9 at 24°C (75°F) was a fast fracture as expected because of the test temperature selected for that purpose. Ultrasonic data did indicate that some stable crack growth occurred before failure, commencing at 145 MPa (21,000 psi) and totalling about 1.27 cm (0.5 in.) just before failure at 185 MPa (26,900 psi). A closeup view of the fractured nozzle in Vessel V-9 is shown in Fig. 7.

The circumferential strain values measured on the outside surfaces of the cylinders of Vessels V-5 and V-9, which are shown plotted in Fig. 8, indicate, by comparison with Fig. 3, that the cylinders of both vessels were fully yielded, but not yet strain hardened, at failure. The strains measured at the inside nozzle corners opposite the flaws, for Vessels V-5 and V-9, are shown plotted in Fig. 9. The nozzle corner strains at failure for Vessels V-5 and V-9 were 6.5% and 8.4%, respectively. Both of these strains are remarkably large compared to the maximum previously measured strain tolerance of the same material for a 4.7 cm (1.87 in.) deep flaw in the cylindrical region of an intermediate test vessel,[14] which was 2%.

The flaw region of Vessel V-5 has not yet been sectioned for posttest examination, but the fracture surfaces containing the original nozzle corner flaw in

Vessel V-9 have been separated, with the results shown in Fig. 10. The original fatigue sharpened crack in Vessel V-9 was very close to the size and shape estimated by ultrasonics before the test[9] (see Fig. 4), and stable crack growth the extent of which can be seen in Fig. 10, did increase the average crack depth by about 1.27 cm (0.5 in.).

Pre- and posttest estimates of the failure strains at the unflawed nozzle corners opposite the flaws in Vessels V-5 and V-9, and the corresponding pressures, were made by ORNL and by others, using several different methods of elastic-plastic fracture analysis, all of a semiempirical nature.[9] All of the direct estimates of the nozzle corner failure strains were low, most by a wide margin. Several such calculations were made by the method of LEFM based on strain, by which the estimated strain is calculated directly by LEFM, and the corresponding pressure is determined from a calculated or a previously measured nonlinear pressure-strain curve. Nozzle corner failure strains calculated by this method, and assuming plane strain toughness conditions, ranged from 0.33% to 0.6%. An equivalent energy calculatic for Vessel V-5, based on small scale steel model test data obtained before the test of Vessel V-5, estimated a failure strain of 1.4%, and a calculation of the failure pressure for Vessel V-5 by the stress concentration method[15] estimated a failure pressure of 189 MPa (27.4 ksi). In addition, graphical estimates of nozzle corner strain tolerances based on surface flawed uniaxial intermediate tensile specimen test data[9] gave estimates of 3.30% for Vessel V-5 and 1.25% for Vessel V-9. Implicitly, the latter three methods did not assume plane strain toughness conditions, and they were more accurate than the methods that did.[9] It was apparent from these calculations, and the test results themselves, that some aspect of nozzle corner geometry was causing the strain tolerances for nozzle corner cracks to be substantially greater than would be expected for the same size cracks in the cylinder of a pressure vessel. In fact, the measured nozzle corner failure strains were closer to the previously

measured failure strains for surface flawed uniaxial tensile bars near and in the upper shelf temperature range.[16] Thus it was clear that the tendency of a plane strain LEFM analysis based on strain to underpredict nozzle corner failure strains by a wide margin, for high toughness conditions, must be due to either an error in the LEFM portion of th. calculation or to the assumption of full transverse restraint around the crack front. The possibility of large errors in the LEFM portion of the analysis was subsequently dismissed because (1) calculations based on several different methods for estimating the LEFM shape factor for nozzle corner cracks had given similar results;[9] (2) the method used by ORNL, based on Derby's epoxy model test data,[17] were confirmed by later photoelastic experiments;[18] and (3) the difference between shape factor values estimated from Derby's data[17] and those based on the solution for an edge crack extending from a hole in a plate[1] were explained by Embly[9,19] as being due to the effects of pressure in the crack, which are experimentally included in the former solution but analytically neglected in the latter. For this reason, the experimentally measured principal strains at the unflawed nozzle corners opposite the flaws in both vessels were examined closely. Both sets of strain readings indicated the occurrence of considerable transverse contraction in the plane of the crack at the nozzle corner, thus implying that full transverse restraint does not exist for nozzle corner cracks at that location, under vessel internal pressure loading. This phenomenon will be discussed further in the section on analysis.

The pretest estimates of failure pressure for Vessel V-5 were based on an elastic-plastic nozzle corner pressure-strain curve calculated by the finite element method.[9] However, this curve proved to be inaccurate with respect to the experimental data obtained for Vessel V-5, because it underestimated the elastic stress concentration factor and overestimated the pressures for given strains in the elastic-plastic range. Therefore, the calculations for Vessel V-9 were

based on the experimentally measured pressure-strain curve for Vessel V-5 shown in Fig. 9, and it was recognized that improved methods for estimating elastic-plastic nozzle corner pressure-strain curves would be required as part of any practical method of fracture analysis for nozzle corner cracks.

ANALYSIS

The experimental data obtained from Intermediate Test Vessels V-5 and V-9 revealed the need for improved accuracy in the representation of several factors involved in the fracture analysis of nozzle corner cracks. Although the linear elastic fracture mechanics relationship between vessel internal pressure and the crack tip stress intensity factor was considered to be satisfactory, the analytical estimate of the nozzle corner pressure-strain curve made before the test of Vessel V-5 was not considered satisfactory, in either the elastic or the elastic-plastic ranges. Furthermore, the reasonableness of any method of extending linear elastic fracture mechanics into the elastic-plastic range for nozzle corner cracks was still undemonstrated, and it was suspected that such a demonstration would require the consideration of transverse restraint effects on toughness as well as the effects of nominal yielding on crack tip behavior per se. Thus the objectives of the analysis developments to be discussed below were principally to develop an improved method for estimating elastic-plastic nozzle corner pressure-strain curves, and to find one or more reasonable methods for considering the combined effects of nominal yielding and partial transverse restraint conditions on the criteria governing the extension of nozzle corner cracks.

Pressure-Strain Curve Estimates

In principle, the nozzle corner pressure-strain curve should be bounded by two tangents, the first representing the initial elastic behavior of the nozzle at low pressures, and the second being the gross yield pressure of the nozzle

region. By comparing the experimentally measured nozzle corner pressure-strain curves for Vessels V-5 and V-9 shown in Fig. 9 with the calculated pressure-strain curve for the vessel cylinders remote from the nozzles shown in Fig. 3, it can be seen that the gross yield pressures indicated by both figures are essentially the same. This is consistent with the assumption that nozzle design by the area replacement method specified by the ASME Code[8] serves to prevent the gross yield pressure of a nozzle region from becoming less than that of the cylinder into which the nozzle is inserted. Therefore, for estimating purposes, the gross yield pressure of a nozzle region designed by the area replacement method will be assumed to be identical to that of the cylinder into which the nozzle is inserted.

Previous comparisons between theory and experiment have shown that the gross yield pressure of an Intermediate Test Vessel cylinder can be closely estimated by the equation

$$p_{GY} = 1.04 \, \ell n \, (r_o/r_i) \, , \qquad (1)$$

where r_o and r_i are the outer and the inner vessel cylinder radii, respectively. In Eq. (1), the factor 1.04 is an empirical factor based on both Intermediate Test Vessel and small scale steel model test data, and the remainder of the equation is based on the Tresca (maximum shear stress) yield criterion. From Table 1, the room temperature yield stresses of the Vessel V-5 and the Vessel V-9 cylinder materials were 500 MPa (72.5 ksi) and 475 MPa (68.9 ksi), respectively. Therefore, assuming test temperature yield stresses of σ_Y = 476 MPa (69.0 ksi) for both vessel cylinders, and using r_o/r_i = 1 4/9, Eq. (1) gives p_{GY} = 182 MPa (26.4 ksi).

Although pretest estimates of the elastic stress concentration factor of the nozzle corners in Vessels V-5 and V-9, based on both elastic finite element analysis[20] and epoxy model strain gage data[17] were approximately 2.9, the experimental strain data obtained from both vessels indicated a value close to 4. The principal stresses calculated from the measured principal strains at low pressures on the unflawed inside nozzle corner of Vessel V-9 are listed in Table 2. These stresses were calculated from Hooke's Law before yielding, and with the aid of the Tresca yield criterion after yielding.[9] Not only is the initial elastic stress concentration factor close to 4, but the intermediate principal stress is initially small and tends to become compressive, eventually equalling the vessel internal pressure after local yielding occurs.

The unexpectedly high values of the nozzle corner stress concentration factor for Vessels V-5 and V-9 were subsequently explained by applying an analysis derived by Van Dyke[21] for calculating the stresses around a circular hole in a thin shallow cylindrical shell. The value of the elastic stress concentration factor of the hole, at the longitudinal plane, is given by Van Dyke's analysis as

$$K_t = 2.5 + \frac{9\pi}{4}\beta^2 , \tag{2}$$

where

$$\beta^2 = \frac{r^2\sqrt{12(1-\nu^2)}}{8r_m t} . \tag{3}$$

In Eq. (3), r is the hole radius, r_m is the cylinder midthickness radius, and t is the cylinder thickness. Applying Eqs. (2) and (3) to the nozzle design shown in Fig. 1, both for the case of an Intermediate Test Vessel cylinder and for a

cylinder of typical reactor vessel dimensions gives the results shown in Table 3. The value of K_t for the nozzle in an Intermediate Test Vessel is 4.16, but the value of K_t for the same nozzle inserted into a typical reactor vessel is only 2.71, because of the influences of the cylinder mean radius and thickness, both of which occur as factors in the denominator of Eq. (3).

Having resolved both the estimates of the gross yield pressure and the elastic stress concentration factor, two semiempirical equations were developed for estimating the elastic-plastic nozzle corner pressure-strain curves of Vessels V-5 and V-9. The initial elastic slopes of these curves were both determined by using the calculated elastic stress concentration factor, and by assuming that the intermediate principal stress was compressive and equal to the vessel internal pressure. Thus the initial slope, M, of the nozzle corner pressure-strain curves were calculated from

$$M = \frac{E}{K_t \left(\frac{r_i}{t}\right) + 2\nu} . \qquad (4)$$

For $E = 2068\ \text{MPa}\cdot\%^{-1}$ ($300\ \text{ksi}\cdot\%^{-1}$), $K_t = 4.16$ and $\nu = 0.3$, Eq. (4) gives $M = 208\ \text{MPa}\cdot\%^{-1}$ ($30.12\ \text{ksi}\cdot\%^{-1}$).

The first semiempirical equation was based on the assumption that the slope of the pressure-strain curve decreases linearly with increasing pressure, and reaches zero at the gross yield pressure. The resulting equation is

$$p = p_{GY}\left(1 - e^{-\frac{M\lambda}{p_{GY}}}\right), \qquad (5)$$

where λ is the nozzle corner strain. For the Intermediate Test Vessel nozzle corners, substituting the values of p_{GY} and M determined from Eqs. (1) and (4)

gives

$$p = 26.4\ (1 - e^{-1.141\lambda})\ , \tag{6}$$

where p is in ksi and λ is in percent. Equation (6) is shown plotted in Fig. 11, which demosntrates that it fits the data from Vessel V-5 with considerable accuracy.

The second semiempirical equation was based on plotting the measured pressure divided by the measured strain versus the measured pressure, for Vessel V-9, from which it was deduced that the two quantities plotted could be approximately related by the equation of an ellipse, namely

$$\left(\frac{p}{M\lambda}\right)^2 + \left(\frac{p}{p_{GY}}\right)^2 = 1\ . \tag{7}$$

Rearranging Eq. (7) gives

$$p = \frac{p_{GY}}{\sqrt{1 + \left(\frac{p_{GY}}{M\lambda}\right)^2}}\ . \tag{8}$$

Again, for the Intermediate Test Vessel nozzle corners, substituting the values of p_{GY} and M obtained from Eqs. (1) and (4) gives

$$p = \frac{26.4}{\sqrt{1 + \left(\frac{0.8765}{\lambda}\right)^2}}\ , \tag{9}$$

where p is in ksi and λ is in percent. Equation (9) is shown plotted in Fig. 11, which demonstrates that it fits the data from Vessel V-9 with equal accuracy. Thus it appears that either or both of the simple semiempirical

expressions discussed above can be used to obtain good estimates of elastic-plastic nozzle corner pressure-strain curves for use in elastic-plastic fracture strength calculations.

Fracture Analyses

Taking into account the tendency of existing plane strain analyses to underpredict nozzle corner flaw strain tolerances, for pressure loading, and the contraction strains measured on the unflawed nozzle corners of Vessels V-5 and V-9, additional nonplain strain analyses were performed for both vessels with considerably improved results. These calculations were performed by two nominally different methods, namely LEFM based on strain and the tangent modulus method. However, these two methods actually have several features in common, and can be used together if desired. Both methods make direct use of the linear elastic fracture mechanics solution for the problem being analyzed. Thus, for the Intermediate Test Vessels with nozzle corner cracks, the experimental curve obtained by Derby[17] for small, thick-walled epoxy model vessels shown in Fig. 12 was used to establish the value of C_n, defined as

$$C_n = \frac{K_I}{\sigma_h \sqrt{\pi a}} . \tag{10}$$

In Eq. (10), σ_h is the nominal cylinder hoop stress, defined by

$$\sigma_h = p\left(\frac{r_i}{t}\right) . \tag{11}$$

In Fig. 12, C_n is given as a function of a/r_z, where r_z is defined by

$$r_z = r_{ni} + r_c\,(1 - 1/\sqrt{2}) , \tag{12}$$

where r_{ni} and r_c are the inside nozzle radius and the inside nozzle corner radius of curvature, respectively. For the Intermediate Test Vessel nozzles, from Fig. 1, r_{ni} = 11.43 cm (4.5 in.) and r_c = 3.81 cm (1.5 in.), so that Eq. (12) gives r_z = 12.55 cm (4.94 in.). For both methods of analysis, the LEFM shape factor based on the peak nozzle corner stress is calculated from

$$C = \frac{C_n}{K_t} , \tag{13}$$

where, for Vessels V-5 and V-9, K_t = 4.16 as determined previously.

In both methods of analysis, $C\sqrt{a}$ is a factor in the resulting expression for the required toughness corresponding to a certain strain and flaw size, and the other factor is a function of strain, uncracked geometry and material properties. The same analytical approximations for the pressure-strain curve are useable in both methods, although one is not needed for the tangent modulus calculations of toughness discussed below.

The representation of the effects of partial transverse restraint on fracture toughness is the same in both methods of analysis. The concept underlying this part of the calculations is that the nominal strain in the direction tangent to the crack front, in the plane of the crack, is the primary agent of transverse restraint.[14] When this strain is zero, plane strain toughness conditions prevail, but when this strain is a contraction, the toughness is elevated above the plane strain toughness. If the transverse contraction strain is approximately equal to or greater than that corresponding to uniaxial tension, the toughness elevation can be estimated from Irwin's empirical formula[22]

$$\frac{K_c}{K_{Ic}} = \sqrt{1 + 1.4\ \beta_{Ic}^2} . \tag{14}$$

For a through crack, β_{Ic} is defined by[22]

$$\beta_{Ic} = \frac{\left(\frac{K_{Ic}}{\sigma_Y}\right)^2}{B} , \tag{15}$$

where B is specimen thickness. However, for a part-through surface crack, an alternate definition,

$$\beta_{Ic} = \frac{\left(\frac{K_{Ic}}{\sigma_Y}\right)^2}{2a} , \tag{16}$$

is used here, in order for the denonimator in the expression for β_{Ic} to retain its identify as twice the distance from the point of greatest transverse restraint on the crack front to the nearest free surface, not including the crack surface.[14] A curve representing Eq. (14) is shown in Fig. 13, in which the abscissa is the reciprocal of β_c, where

$$\beta_c = \frac{\left(\frac{K_c}{\sigma_Y}\right)^2}{B} \text{ or } \frac{\left(\frac{K_c}{\sigma_Y}\right)^2}{2a} , \tag{17}$$

as appropriate. For large values of β_c, the curve shown in Fig. 13 can be closely approximated by

$$\frac{K_c}{K_{Ic}} = 1.058\ \beta_c^{1/3} . \tag{18}$$

Although the above method for considering transverse restraint ~~efforts~~ EFFECTS sometimes involves applying Eq. (14) at rather large values of β_c, a previous analysis of large surface cracked Intermediate Tensile Specimens has shown, by accurate results, that such an application is empirically justified.[14]

One difference between the two methods of analysis, as applied below, is that stable crack growth is neglected in the first analysis, but considered in the second. In estimating failure strains by the method of LEFM based on strain, the original crack sizes are used. Nevertheless, the results are slightly conservative. In calculating the toughnesses corresponding to given nozzle corner strain levels by the tangent modulus method, actual crack sizes are used, and again the results are quite reasonable. It follows that stable crack growth should be considered when estimating failure strains by the latter method, in order to avoid unconservative results.

The estimate of nozzle corner failure strains by the method of LEFM based on strain begins with the combination of Eqs. (10) and (11), rearranged and symbolically changed to read

$$p_f^* = \frac{K_{Ic}}{C_n \left(\frac{r_i}{t}\right) \sqrt{\pi a}} . \tag{19}$$

In Eq. (19), p_f^* is the elastically calculated failure pressure and K_{Ic} is the plane strain fracture toughness. The failure strain for plane strain conditions is calculated from

$$\lambda_{fo} = \frac{p_f^*}{M} . \tag{20}$$

The failure strain for nonplane strain conditions is then calculated from

$$\lambda_f = \left(\frac{K_c}{K_{Ic}}\right)\lambda_{fo} \,, \tag{21}$$

where the ratio (K_c/K_{Ic}) is obtained from Eq. (14). The estimated failure PRESSURE is then calculated from Eq. (9). The results are shown in Table 4. The three values of failure strain and pressure listed for Vessel V-9 are those corresponding to the three measured fracture toughness values listed in the upper part of the table. For Vessel V-5, the calculated failure strain and failure pressure are only slightly conservative, and the same is true of the strain and pressure corresponding to the maximum fracture toughness value measured for Vessel V-9. Noting the large differences between the plane strain and the nonplane strain estimates of failure strain for both vessels, it is clear that considering the effects of transverse restraint is essential to the accuracy of the analysis.

The calculations of the plane strain fracture toughnesses corresponding to given measured values of nozzle corner strain and flaw size by the tangent modulus method were based on the directly measured flaw size at failure for Vessel V-9 (see Fig. 10), and the last ultrasonically measured flaw size in Vessel V-5 before the pressure began to decrease.[9] Note that the flaw in Vessel V-5 was 8.4 cm (3.3 in.) deep at a pressure of 183 MPa (26.5 ksi), and therefore underwent approximately 12.7 cm (5 in.) of stable crack growth during the last 0.7 MPa (100 psi) rise in pressure.

Because of the steep strain gradient in the nozzle corner region, the tangent modulus equations for the case of bending[14] were used for these toughness calculations. The derivation of these equations is given in Appendix H of Ref. 14. Briefly, this method of analysis is based on the Neuber equation for

inelastic stress and strain concentration factors,

$$K_\sigma K_\varepsilon = K_t^2 \ , \tag{22}$$

written in incremental form and then rearranged so that the increment in the notch ductility factor $d\varepsilon\sqrt{\rho}$, where ε is notch root strain and ρ is notch root radius, appears on the lefthand side of the equation and only measurable quantities appear on the righthand side. For a trilinearized stress-strain curve and the case of bending, with the applied strain in the strain hardening range, the notch ductility factor increments were calculated from the equations given below.[14] For the elastic range,

$$\Delta\varepsilon\sqrt{\rho} = 2C\sqrt{a}\sqrt{E/E_s}\ \lambda_Y \ . \tag{23}$$

For the transition range,

$$\Delta\varepsilon\sqrt{\rho} = 4C\sqrt{a}\sqrt{E/E_s}\ (\sqrt{\lambda_s\lambda_Y} - \lambda_Y) \ . \tag{24}$$

For the strain hardening range,

$$\Delta\varepsilon\sqrt{\rho} = 2C\sqrt{a}\left\{\sqrt{\lambda_f(\lambda_f + \lambda_d)} - \sqrt{\lambda_s(\lambda_s + \lambda_d)} + \lambda_d\ \ell n\left[\frac{\sqrt{\lambda_f} + \sqrt{\lambda_f + \lambda_d}}{\sqrt{\lambda_s} + \sqrt{\lambda_s + \lambda_d}}\right]\right\}, \tag{25}$$

where

$$\lambda_d = \frac{\sigma_Y}{E_s} - \lambda_s \ . \tag{26}$$

In Eqs. (23) through (26), λ_Y is the yield strain, λ_s is the strain at the onset of strain hardening, λ_f is the applied or failure strain, E is the elastic modulus, and E_s is the strain-hardening tangent modulus. For both vessels, the value

of E_s was taken as 20.7 MPa·%$^{-1}$ (3.0 ksi·%$^{-1}$), and λ_s was taken as 1.2%. The total values of $\varepsilon_f\sqrt{\rho}$ were calculated by adding the values obtained from Eqs. (23), (24), and (25), and the values of K_c/σ_Y were then obtained from[14]

$$\frac{K_c}{\sigma_Y} = \left(\frac{\sqrt{\pi}}{20\lambda_Y}\right)\varepsilon_f\sqrt{\rho} \ . \tag{27}$$

The values of K_{Ic}/σ_Y were then obtained by dividing the results of Eq. (27) by the values of K_c/K_{Ic}, obtained from either Fig. 13 or Eq. (18). The resulting toughness values for both vessels are listed in the lower part of Table 4. Both plane strain toughness values compare well with the measured values for the two nozzle materials. The nonplane strain toughness ratios, K_c/σ_Y, may look high, but the calculated crack tip opening displacements listed at the bottom of Table 4, as calculated from

$$\delta_c = \frac{\sigma_Y}{E}\left(\frac{K_c}{\sigma_Y}\right)^2 \ , \tag{28}$$

are both only reasonably smaller than the measured crack mouth opening displacements just prior to maximum load,[9] which is to be expected for cracks located in steep nominal strain gradients. Thus the necessity for considering partial transverse restraint effects for nozzle corner cracks under vessel internal pressure loading is again confirmed.

Table 1. Reference data for analysis of HSST Program Intermediate Test Vessels V-5 and V-9

	Vessel V-5	Vessel V-9
Nozzle material	A508, class 2 forging steel, base metal	A508, class 2 forging steel, base metal
Nozzle NDT temperature	−12°C (+10°F) (assumed, based on V-1 data)	−12°C (+10°F) (assumed, based on V-1 data)
Vessel test temperature	88°C (+190°F)	24°C (+75°F)
Expected fatigue-sharpened flaw depth at inside nozzle corner	3.05 cm (1.2 in.)	3.05 cm (1.2 in.)
Tensile properties of nozzle material at 24°C (75°F)		
Yield stress	425 MPa (61.6 ksi)	474 MPa (68.8 ksi)
Ultimate stress	553 MPa (80.2 ksi)	609 MPa (88.3 ksi)
Strain at maximum load	8.9%	9.0%
Total elongation	16.8%	18.1%
Gage length	3.175 cm (1.250 in.)	3.175 cm (1.250 in.)
Reduction in area	68.3%	70.3%
Original specimen diam.	0.4509 cm (0.1775 in.)	0.4509 cm (0.1775 in.)
Room temperature tensile and drop-weight NDT properties of cylinder material		
Material	A508, class 2	A533, grade B, class 1
Yield stress	500 MPa (72.5 ksi)	475 MPa (68.9 ksi)
Ultimate stress	654 MPa (94.8 ksi)	574 MPa (83.3 ksi)
Total elongation	Not reported	28%
Gage length	Not reported	5.08 cm (2.0 in.)
NDT temperature	Not reported	−51°C (−60°F)
Nozzle dimensions		
Inside radius	11.43 cm (4.5 in.)	11.43 cm (4.5 in.)
Thickness	15.24 cm (6.0 in.)	15.24 cm (6.0 in.)
Cylinder dimensions		
Inside diameter	68.58 cm (27.0 in.)	68.58 cm (27.0 in.)
Thickness	15.24 cm (6.0 in.)	15.24 cm (6.0 in.)
Charpy V-notch impact energy of nozzle material at 24°C (75°F)	No data	90.8 J (67 ft-lb)

Table 2. Principal stress and elastic stress-concentration factor values at the inside unflawed nozzle corner of intermediate test vessel V-9, calculated from experimental strain data

Pressure [MPa (ksi)]	Stress (MPa)			Remarks	K_t
	σ_1	σ_2	σ_3		
6.9 (1.0)	63	0.4	−6.9	Elastic	4.05
13.8 (2.0)	134	3.5	−13.8	Elastic	4.33
34.5 (5.0)	302	6.2	−34.5	Elastic	3.89
55.2 (8.0)	419	−9.9	−55.2	Yield	
68.9 (10.0)	405	−47.8	−68.9	Yield	
75.8 (11.0)	399	−75.8	−75.8	Yield (corner)	

Table 3. Stress-concentration factor estimates for identical nozzles in an intermediate test vessel and a reference calculational model of typical PWR vessel design

Term	Intermediate test vessel with nozzle	Reference calculational model of PWR vessel
Nozzle mean radius r	19.05 cm (7.5 in.)	19.05 cm (7.5 in.)
Cylinder mean radius r_m	41.91 cm (16.5 in.)	229.24 cm (90.25 in.)
Cylinder thickness	15.24 cm (6.0 in.)	21.59 cm (8.5 in.)
β	0.484	0.174
K_t	4.16	2.71

Table 4. Calculated failure strains and fracture toughness values for HSST Program Intermediate Test Vessels V-5 and V-9 with nozzle corner cracks

	Vessel V-5	Vessel V-9
Test conditions, material properties and test results		
Test temperature	88°C (190°F)	24°C (75°F)
Nozzle yield stress	425 MPa (61.6 ksi)	474 MPa (68.8 ksi)
Initial crack depth	3.05 cm (1.2 in.)	3.05 cm (1.2 in.)
Measured nozzle corner failure strain	6.5%	8.4%
Measured fracture toughness	265 $MN \cdot m^{-3/2}$ (241 ksi $\sqrt{in.}$)	159 $MN \cdot m^{-3/2}$ (145 ksi $\sqrt{in.}$) 220 $MN \cdot m^{-3/2}$ (200 ksi $\sqrt{in.}$) 298 $MN \cdot m^{-3/2}$ (271 ksi $\sqrt{in.}$)
Calculated failure strains and pressures by LEFM based on strain		
Flaw size, a	3.05 cm (1.2 in.)	3.05 cm (1.2 in.)
Flaw depth ratio, a/r_z	0.243	0.243
Shape factor, C_n	2.5	2.5
Toughness ratio, K_c/K_{Ic}	7.61	2.41, 4.28, 7.71
Calculated failure strains		
λ_{fo} (plane strain)	0.73%	0.44%, 0.61%, 0.82%
λ_f (nonplane strain)	5.6%	1.1%, 2.6%, 6.4%
Calculated failure pressure	180 MPa (26.1 ksi)	142 MPa (20.6 ksi) 172 MPa (25.0 ksi) 181 MPa (26.2 ksi)
Fracture toughness calculations by the tangent modulus method		
Pressure, p	183 MPa (26.5 ksi)	185 MPa (26.9 ksi)
Nozzle corner strain, λ	5.2%	8.4%
Flaw depth, a	8.4 cm (3.3 in.)	4.50 cm (1.77 in.)
Flaw depth ratio, a/r_z	0.668	0.358
Shape factors		
C_n	1.79	2.18
C	0.430	0.524
Toughness ratios		
K_c/σ_Y	20.51 $\sqrt{cm}$ (12.87 $\sqrt{in.}$)	22.82 $\sqrt{cm}$ (14.32 $\sqrt{in.}$)
K_c/K_{Ic}	3.10	4.09
K_{Ic}/σ_Y	6.23 $\sqrt{cm}$ (4.16 $\sqrt{in.}$)	5.58 $\sqrt{cm}$ (3.50 $\sqrt{in.}$)
Fracture toughness, K_{Ic}	281 $MN \cdot m^{-3/2}$ (256 ksi $\sqrt{in.}$)	265 $MN \cdot m^{-3/2}$ (241 ksi $\sqrt{in.}$)
Crack opening displacement, δ_c	8.6 mm (0.34 in.)	11.9 mm (0.47 in.)

References

1. PVRC Ad Hoc Group on Toughness Requirements, *PVRC Recommendations on Toughness Requirements for Ferritic Materials*, WRC Bulletin 175, Welding Research Council, August 1972.

2. ASTM Task Group E24.01.09, *Recommended Procedure for J_{Ic} Determination*, draft document dated Mar. 1, 1977.

3. Shih, C. F., et al., *Methodology for Plastic Fracture*, fourth quarterly progress report to EPRI, SRD-77-092, General Electric Company, Schenectady, New York, June 6, 1977.

4. Paris, P. C., Tada, H., Zahoor, A., and Ernst, H., "Instability of the Tearing Mode of Elastic-Plastic Crack Growth," paper to be presented at the *ASTM Symposium on Elastic-Plastic Fracture, Atlanta, Ga., Nov. 16-18, 1977.*

5. Pickett, A. G. and Grigory, S. C., *Trans. ASME, J. Basic Engineering* 89(C), 858–870 (December 1967).

6. *Report to Congress on Abnormal Occurrences, October–December 1976*, NUREG-0090-6, U.S. Nuclear Regulatory Commission, June 1977.

7. Mager, T.R., et al., *The Effect of Low Frequencies on the Fatigue Crack Growth Characteristics of A533, Grade B, Class 1 Plate in an Environment of High-Temperature Primary Grade Nuclear Reactor Water*, WCAP-8256, Westinghouse Electric Corp., Pittsburgh, Pa., December 1973.

8. ASME Boiler and Pressure Vessel Code, Section III, Division I, *Nuclear Power Plant Components*, 1974 edition.

9. Merkle, J. G., Robinson, G. C., Holz, P. P., and Smith, J. E., *Test of 6-In.-Thick Pressure Vessels. Series 4: Intermediate Test Vessels V-5 and V-9 With Inside Nozzle Corner Cracks*, ORNL/NUREG-7, Oak Ridge National Laboratory, Oak Ridge, Tennessee, August 1977.

10. Mager, T. R., Yanichko, S. E., and Singer, L. R., *Fracture Toughness Characterization of HSST Intermediate Pressure Vessel Material*, WCAP-8456, Westinghouse Electric Corp., Pittsburgh, Pa., December 1974.

11. Witt, F. J. and Mager, T. R., *A Procedure for Determining Bounding Values on Fracture Toughness K_{Ic} at Any Temperature*, ORNL-TM-3894, Oak Ridge National Laboratory, Oak Ridge, Tennessee, October 1972.

12. Merkle, J. G. and Corten, H. T., *ASME J. Pressure Vessel Technology*, 286–292 (November 1974).

13. Merkle, J. G., et al., *Test of 6-In.-Thick Pressure Vessels. Series 3: Intermediate Test Vessel V-7*, ORNL/NUREG-1, Oak Ridge National Laboratory, Oak Ridge, Tennessee, August 1976.

14. Bryan, R. H., et al., *Test of 6-Inch-Thick Pressure Vessels. Series 2: Intermediate Test Vessels V-3, V-4 and V-6*, ORNL-5059, Oak Ridge National Laboratory, Oak Ridge, Tennessee, November 1975.

15. Irvine, W. H., *A Stress Concentration Theory of Fracture and Its Relationship to Linear Elastic Fracture Mechanics*, SRD R21, UKAEA Safety and Reliability Directorate, Culcheth, Warrington, Lancashire, April 1973.

16. Grigory, S. C., *Nuclear Engineering and Design* 17(1), 161–169 (1971).

17. Derby, R. W., *Exp. Mech.* 12(12), 580–584 (1972).

18. Smith, C. W., Jolles, M., and Peters, W. H., *Stress Intensities for Nozzle Cracks in Reactor Vessels*, VPI-E-76-25, Virginia Polytechnic Institute and State University, Blacksburg, Va., November 1976.

19. Embly, G. T., *Stress Intensity Factors for Nozzle Corner Flaws*, Knolls Atomic Power Laboratory, Schenectady, New York, draft dated July 1974 (to be published).

20. Krishnamurthy, N., paper G 2/7, Vol. 4, *Proc. First Int. Conf. on Structural Mechanics in Reactor Technology, Berlin, 1971.*

21. Van Dyke, P., *AIAA Journal* 3(9), 1733–1742 (1965).

22. Irwin, G. R., Krafft, J. M., Paris, P. C., and Wells, A. A., *Basic Aspects of Crack Growth and Fracture*, NRL Report 6598, U.S. Naval Research Laboratory, Washington, D.C., November 21, 1967.

Figure Captions

Fig. 1. Design dimensions for intermediate test vessel with 22.86 cm (9 in.) ID test nozzle (1 in. = 2.54 cm).

Fig. 2. General view of two HSST program intermediate test vessels, showing bolted-on closure head used for all vessels and welded-in nozzle used for vessels V-5 and V-9.

Fig. 3. Calculated pressure vs outside circumferential strain for cylindrical region of intermediate test vessel (1 ksi = 6.8948 MPa).

Fig. 4. Pretest estimate of fatigue crack front position in the inside nozzle corner of intermediate test vessel V-9, based on ultrasonic data.

Fig. 5. Static and dynamic K_{Icd} values for vessel V-9 nozzle material [1 in. = 2.54 cm; 1 ksi $\sqrt{\text{in.}}$ = 1.0988 $MN \cdot m^{-3/2}$; °C = 5/9 (°F − 32)].

Fig. 6. Closeup view of leak point adjacent to ultrasonic base block on nozzle of vessel V-5 (arrow shows flaw penetration to surface).

Fig. 7. Closeup view of fractured nozzle in vessel V-9; test temperature was 24°C (75°F).

Fig. 8. Pressure vs outside circumferential strain in vessel cylinder for intermediate test vessels V-5 and V-9 (1 psi = 6895 Pa).

Fig. 9. Pressure vs inside uncracked nozzle corner circumferential strain for intermediate test vessels V-5 and V-9 (1 psi = 6895 Pa).

Fig. 10. Closeup view of flaw in fractured nozzle of intermediate test vessel V-9.

Fig. 11. Comparison of calculated and measured nozzle corner pressure-strain curves for intermediate test vessels V-5 and V-9.

Fig. 12. Summary of experimental results obtained from ORNL nozzle corner crack epoxy model fracture tests,[17] and comparison with hole in flat plate approximation.[1]

Figure Captions (continued)

Fig. 13. Curve for estimating toughness elevation due to less than full transverse restraint, based on the Irwin β_{Ic} correction.

Nomenclature

a	Crack depth, cm, (in.)
B	Plate thickness, cm, (in.)
C	LEFM shape factor based on local stress, dimensionless
C_n	LEFM shape factor based on nominal stress, dimensionless
E	Modulus of elasticity, MPa, (ksi)
E_s	Strain hardening tangent modulus, MPa, (ksi)
K_I	Mode I elastic crack tip stress intensity factor, $MN \cdot m^{-3/2}$, (ksi $\sqrt{in.}$)
K_{Ic}	Plane strain fracture toughness, $MN \cdot m^{-3/2}$, (ksi $\sqrt{in.}$)
K_{Icd}	Fracture toughness measured with a specimen of thickness d and calculated from the test data by the equivalent energy procedure, $MN \cdot m^{-3/2}$, (ksi $\sqrt{in.}$)
K_c	Nonplane strain fracture toughness, $MN \cdot m^{-3/2}$, (ksi $\sqrt{in.}$)
K_t	Elastic stress concentration factor, dimensionless
K_ε	Inelastic strain concentration factor, dimensionless
K_σ	Inelastic stress concentration factor, dimensionless
M	Initial slope of the pressure-strain curve, MPa, (ksi)
p	Pressure, MPa, (ksi)
p_f^*	Elastically calculated failure pressure, MPa, (ksi)
p_{GY}	Gross yield pressure, MPa, (ksi)
r_c	Nozzle corner radius of curvature, cm, (in.)
r_i	Inside radius of vessel cylinder, cm, (in.)
r_m	Midthickness radius of vessel cylinder, cm, (in.)
r_{ni}	Inside radius of nozzle, cm, (in.)
r_o	Outside radius of vessel cylinder, cm, (in.)
r_z	Effective nozzle radius, cm, (in.)

t	Thickness of vessel cylinder, cm, (in.)
β	Shell analysis parameter, dimensionless
β_{Ic}	Plane strain plastic zone size parameter, dimensionless
β_c	Nonplane strain plastic zone size parameter, dimensionless
δ_c	Calculated crack opening displacement, mm, (in.)
ε	Notch root strain, dimensionless
λ	Applied strain, dimensionless
λ_d	Stress-strain parameter, dimensionless
λ_f	Failure strain, dimensionless
λ_{fo}	Calculated failure strain for plane strain conditions, dimensionless
λ_s	Strain at the onset of strain hardening, dimensionless
λ_Y	Yield strain, dimensionless
ν	Poisson's ratio, dimensionless
ρ	Notch root radius, cm, (in.)
σ_h	Nominal hoop stress in vessel cylinder, MPa, (ksi)
σ_Y	Yield stress, MPa, (ksi)

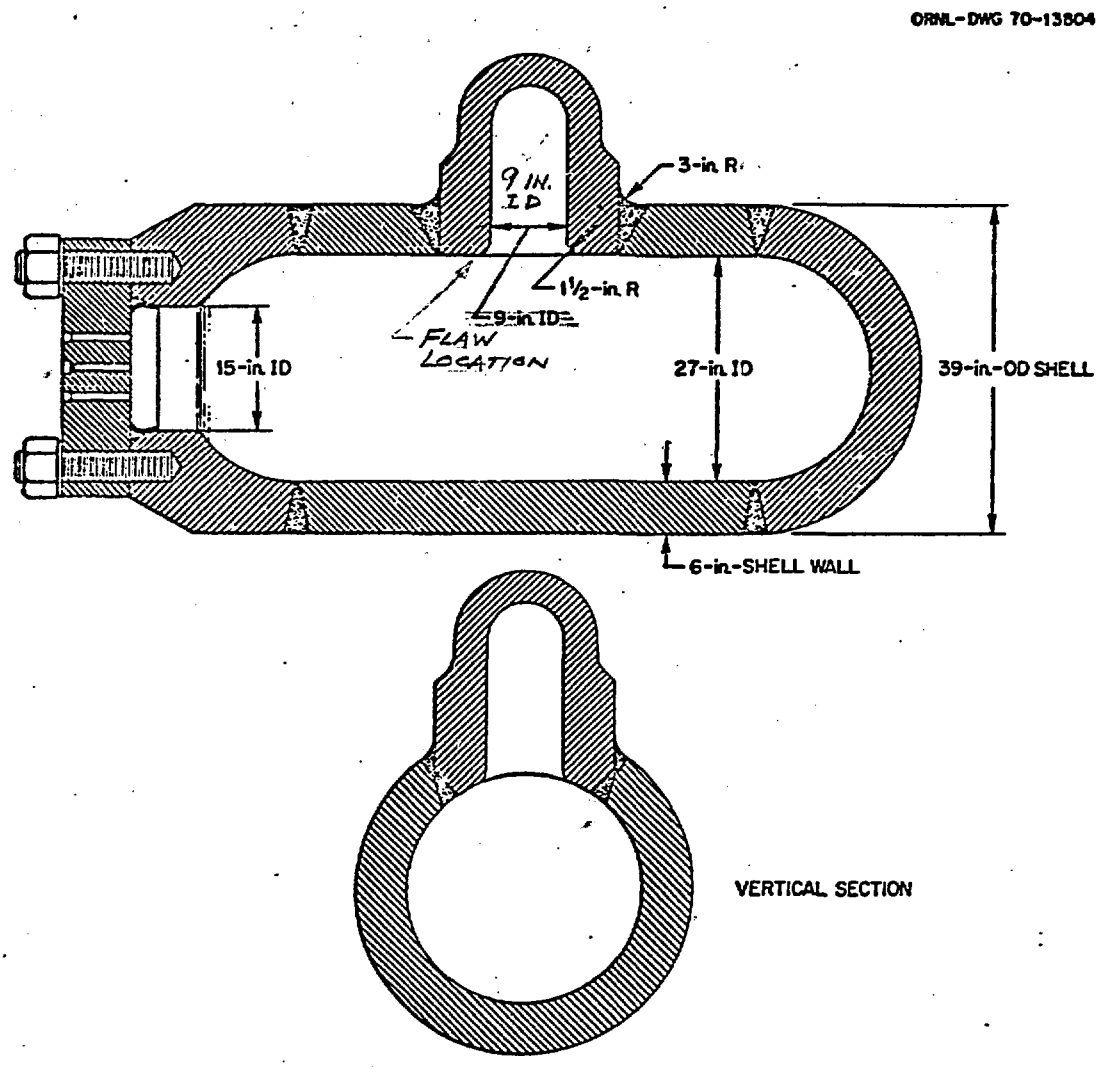

Intermediate test cylindrical vessel with 9-in.-ID test nozzle.

Figure 1

FIG. 1

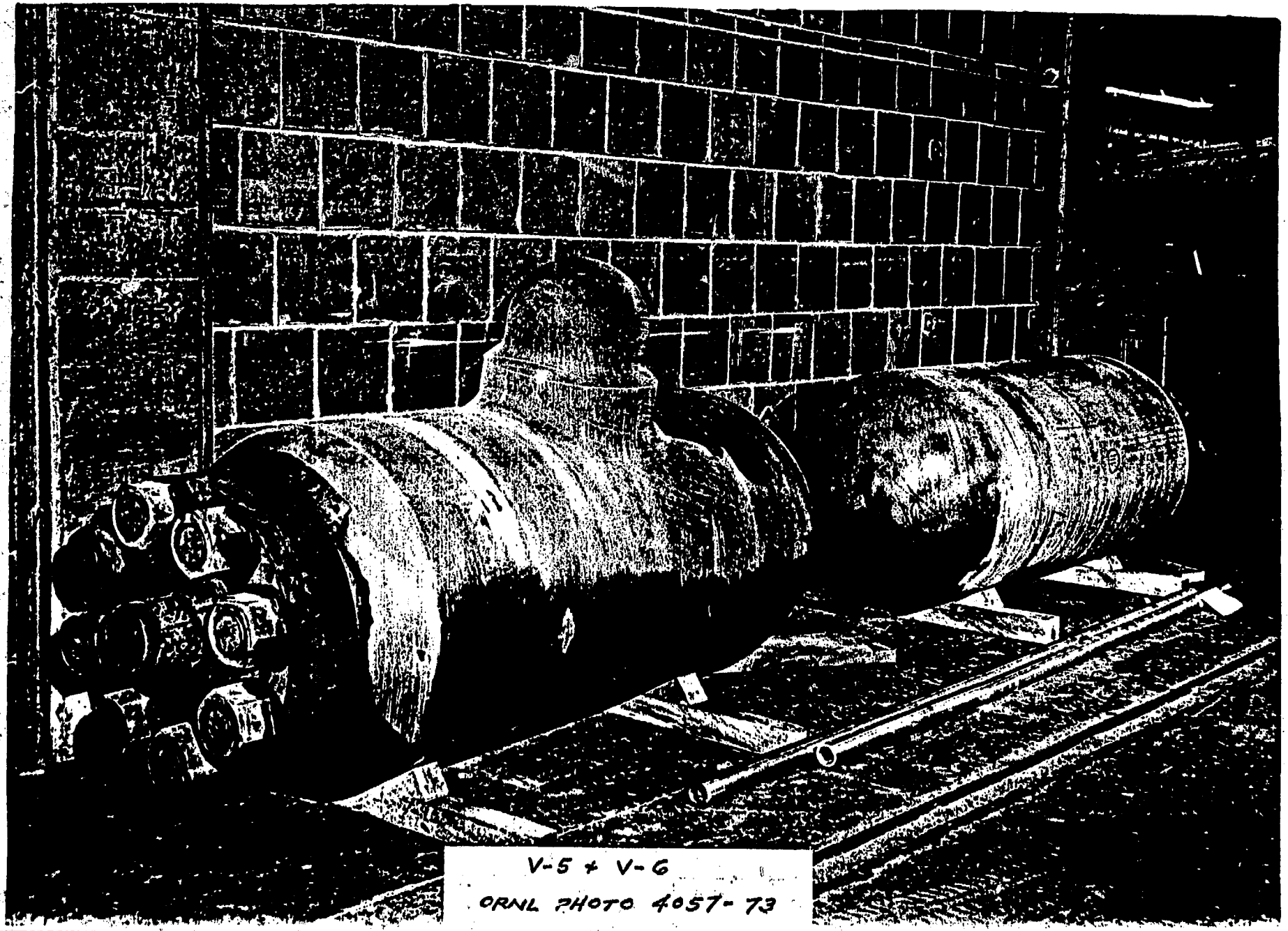

V-5 + V-6
ORNL PHOTO 4057-73

Fig 2

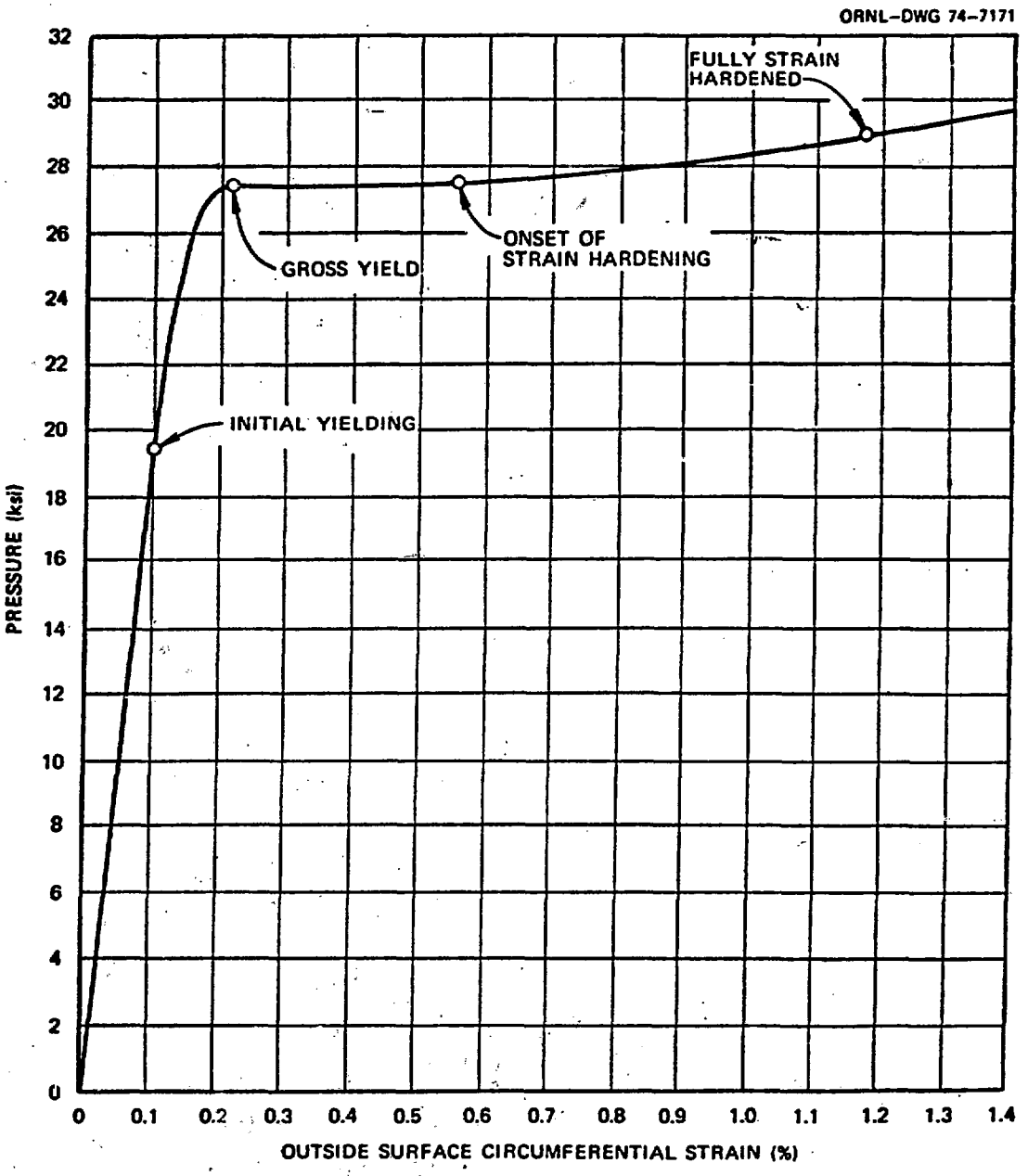

Fig. 8. Calculated pressure vs outside circumferential strain curve for intermediate test vessel.

FIG. 3

PRELIMINARY CALCULATIONS FOR IVT-9

FLAW DEPTH

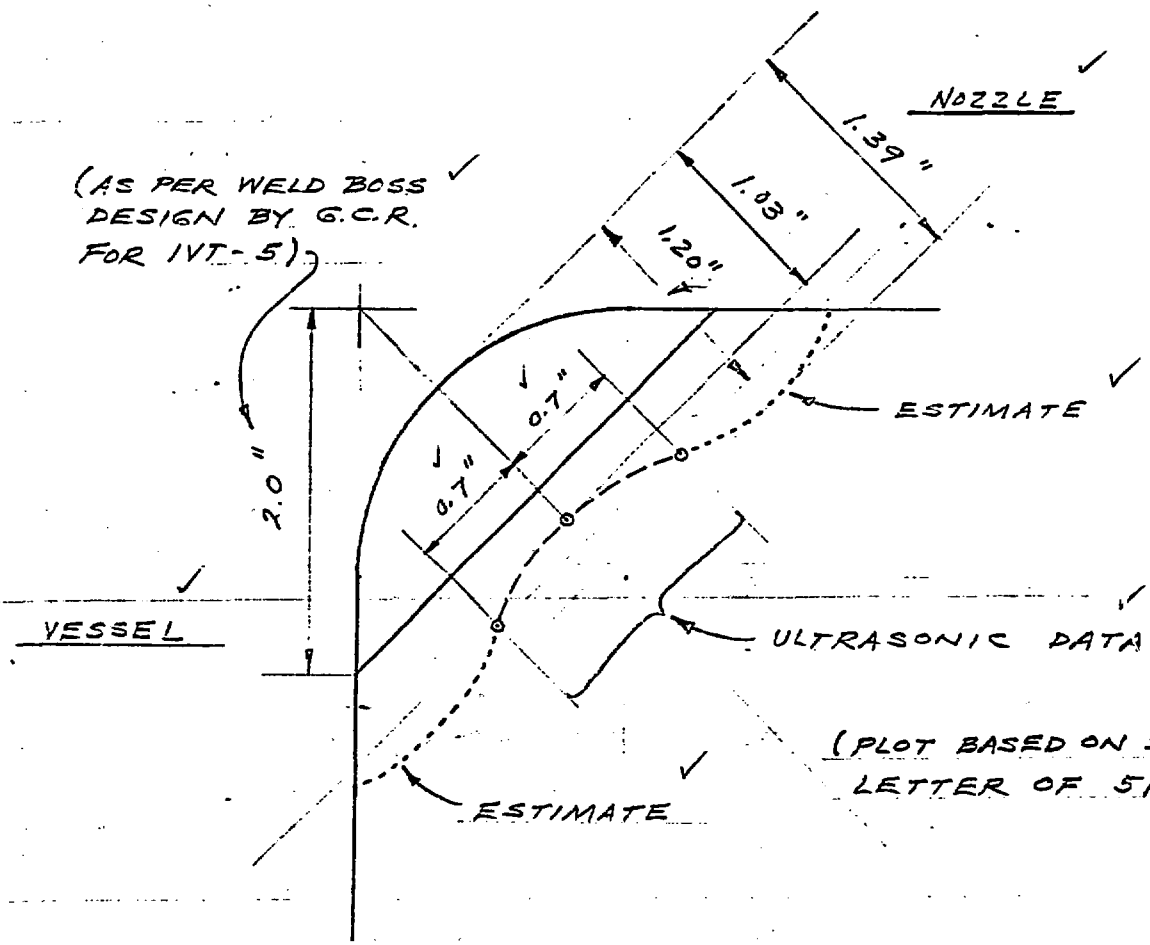

USE A NOMINAL CRACK DEPTH, $a = 1.2"$
(SAME AS IVT-5)

NOMINAL STRESS DISTRIBUTION IN THE CYLINDER

$\sigma_{\theta i} = 2.84\ p$
$\sigma_{\theta o} = 1.84\ p$
} ORNL-4895, p. 209

$(1.10)(2.84) = 3.12$ FIG. 4 (p. 380)

$\sigma_{\theta i}$ IS NOT MORE THAN 10% ABOVE THE NOMINAL VALUE AT A DISTANCE OF 14" FROM THE NOZZLE AXIS. (MEDIUM MESH, p. 380)

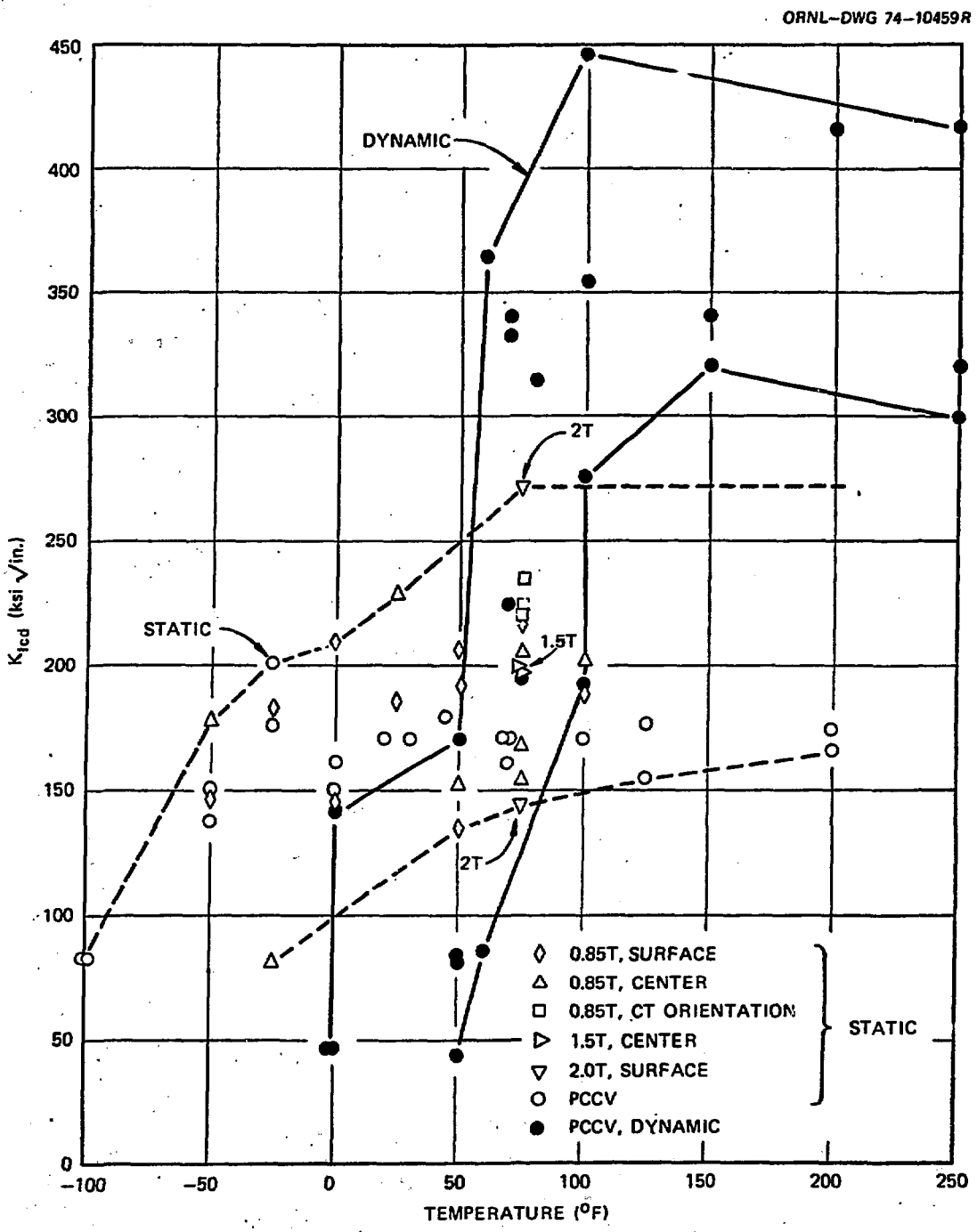

Fig. 2.20. Static and dynamic K_{Icd} values for vessel V-9 nozzle material [1 in. = 2.54 cm; 1 ksi$\sqrt{\text{in.}}$ = 1.0988 MN·m$^{-3/2}$; °C = $\frac{5}{9}$(°F − 32)].

FIG. 5

Fig. 4.13. Closeup view of leak point adjacent to ultrasonic base block on nozzle of vessel V-5 (arrow shows flaw penetration to surface).

FIG. 6

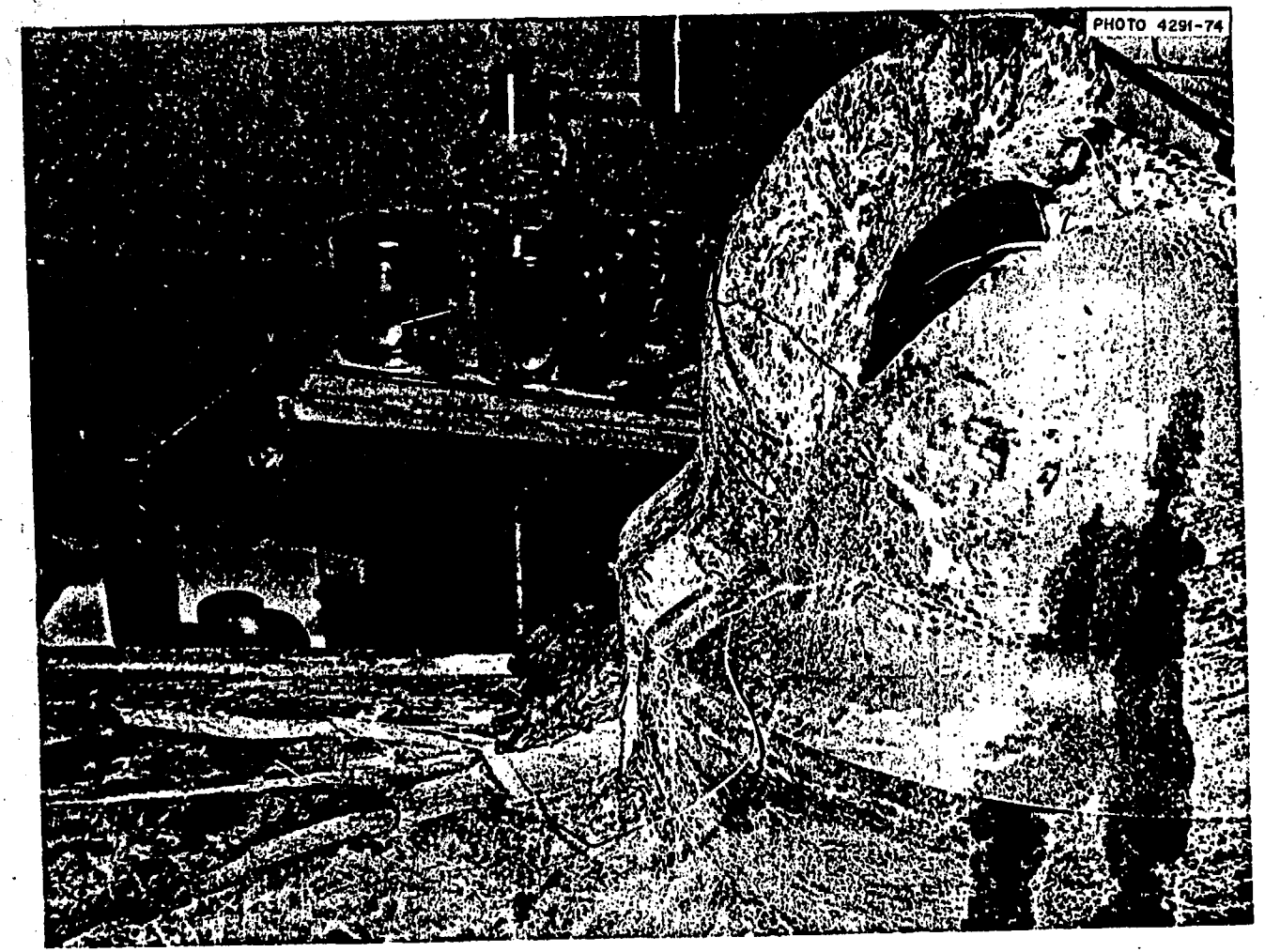

Fig. 4.21. Close-up view of fractured nozzle in vessel V-9; test temperature was 24°C (75°F).

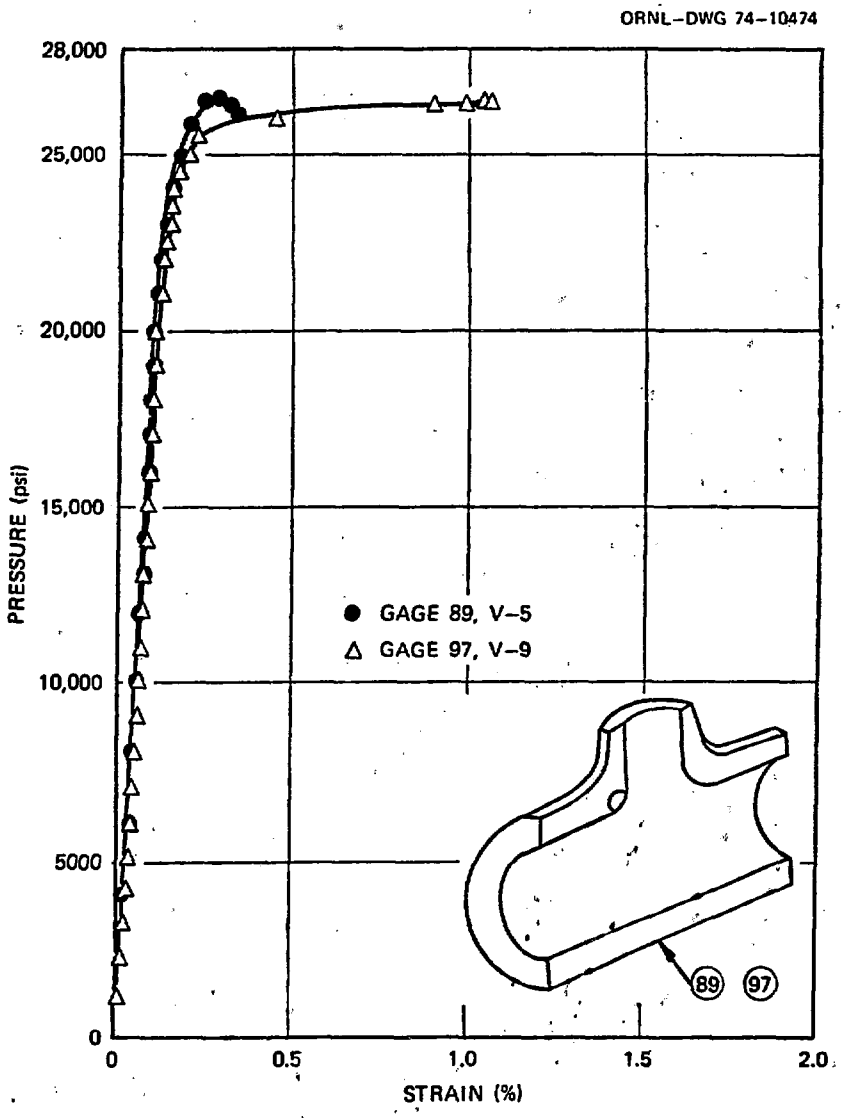

Fig. 4.23. Pressure vs outside circumferential strain in vessel cylinder for intermediate vessels V-5 and V-9 (1 psi = 6895 Pa).

FIG 8

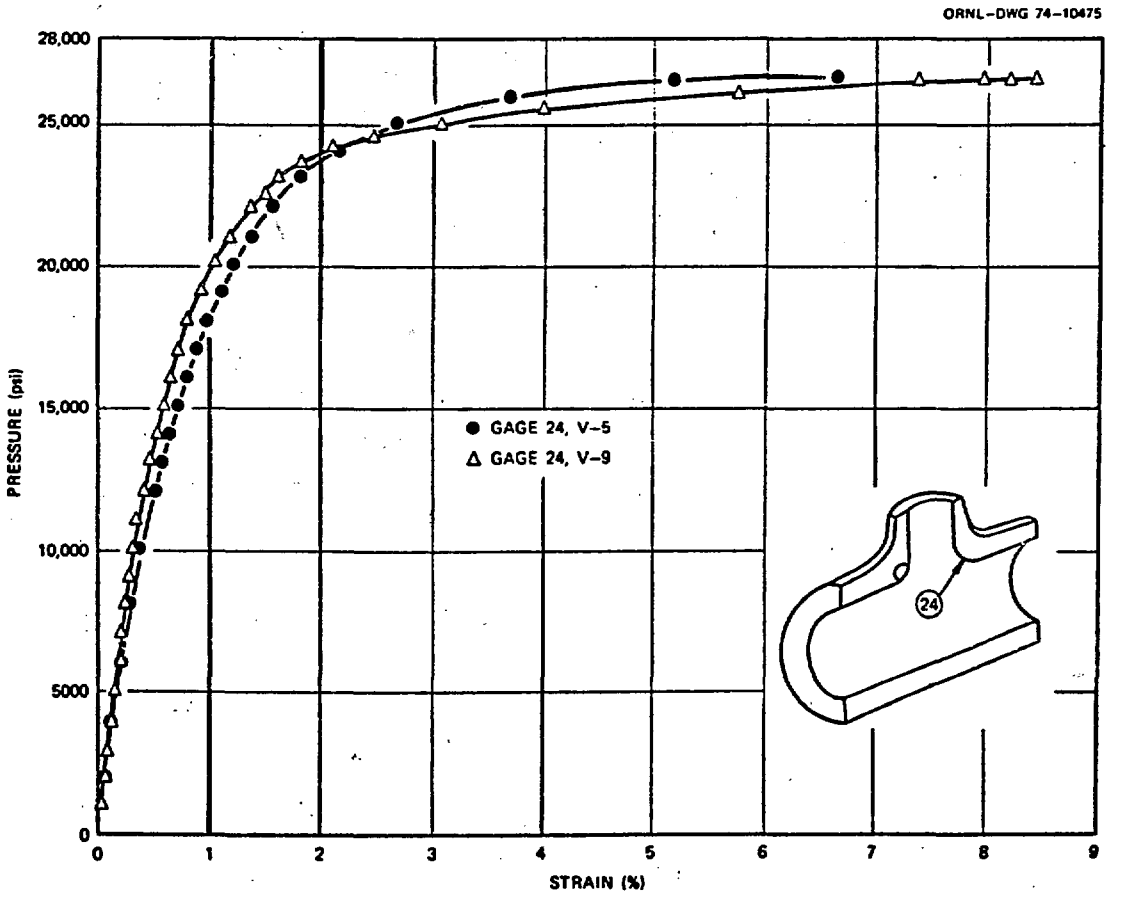

Fig. 4.24. Pressure vs inside uncracked nozzle corner circumferential strain for intermediate test vessels V-5 and V-9 (1 psi = 6895 Pa).

Fig. 9

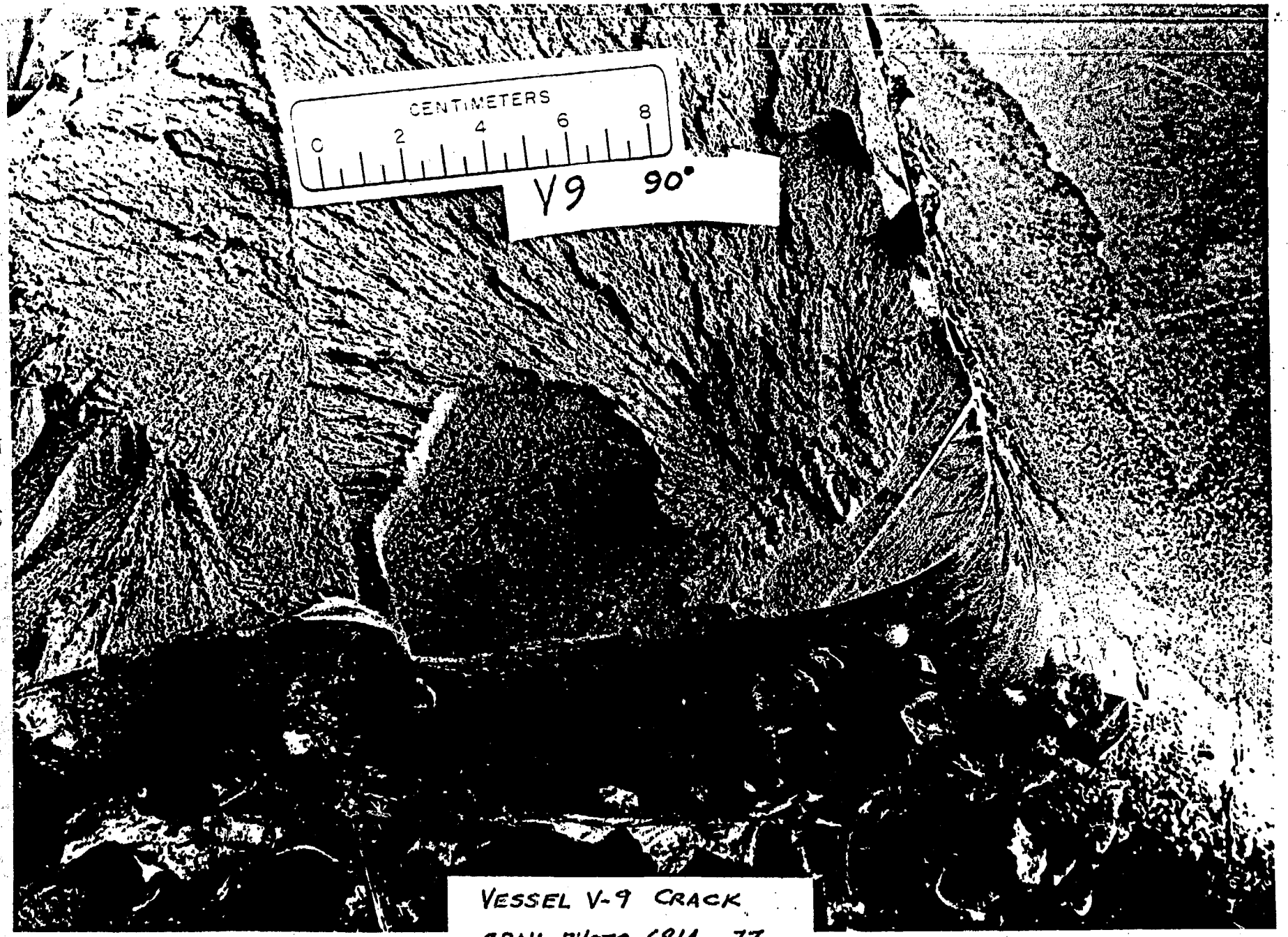

VESSEL V-9 CRACK
ORNL PHOTO 6914-77

FIG. 10

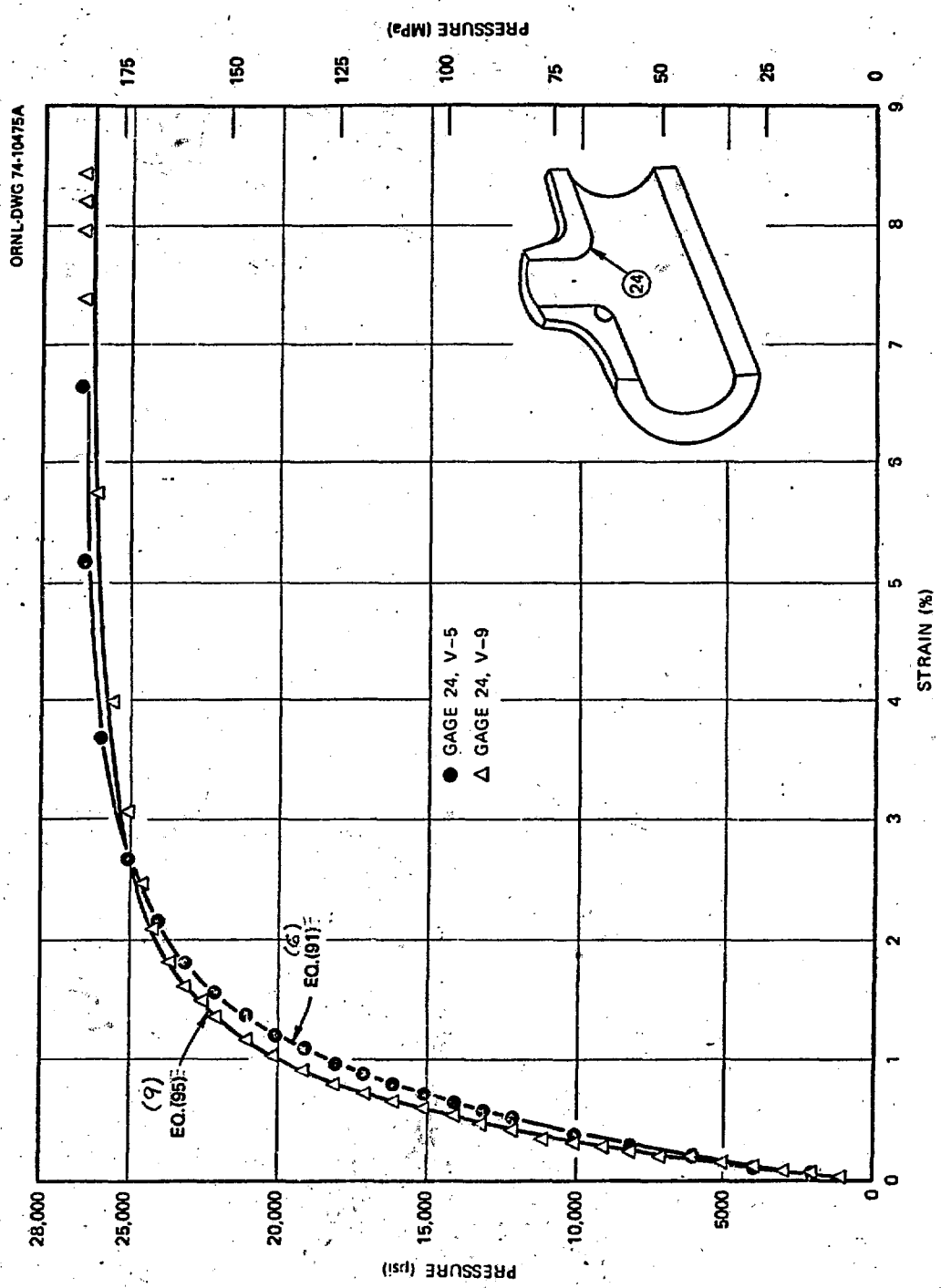

Fig. 5.33. Comparison of calculated and measured nozzle corner pressure-strain curves for intermediate test vessels V-5 and V-9.

FIG. 11

USE FIG. "A-15"

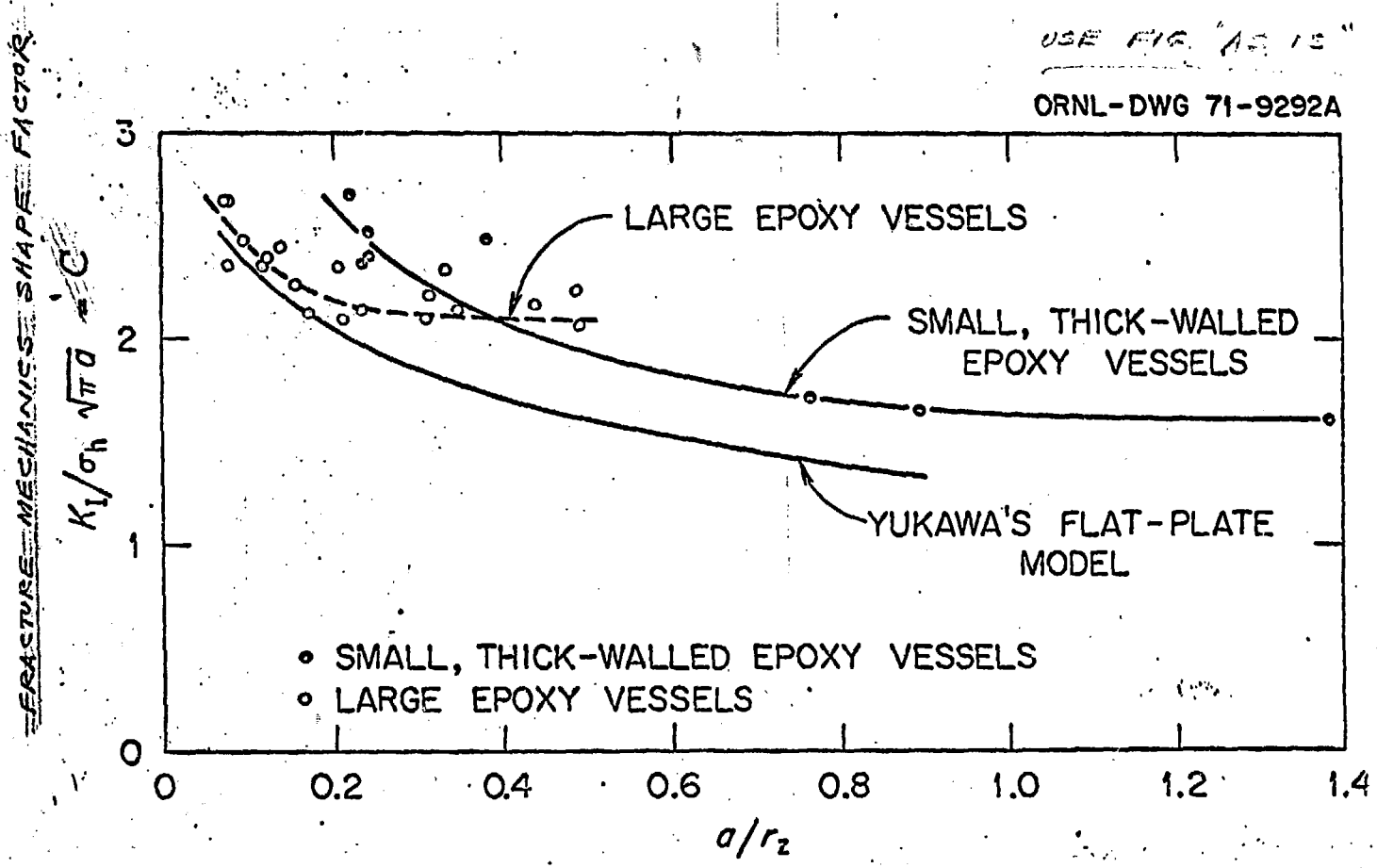

FIG. 12

(THE ORIGINAL DRAWING FOR THIS FIGURE IS FILED UNDER "ORIGINAL FIGURES").

THIS FIGURE EXISTS

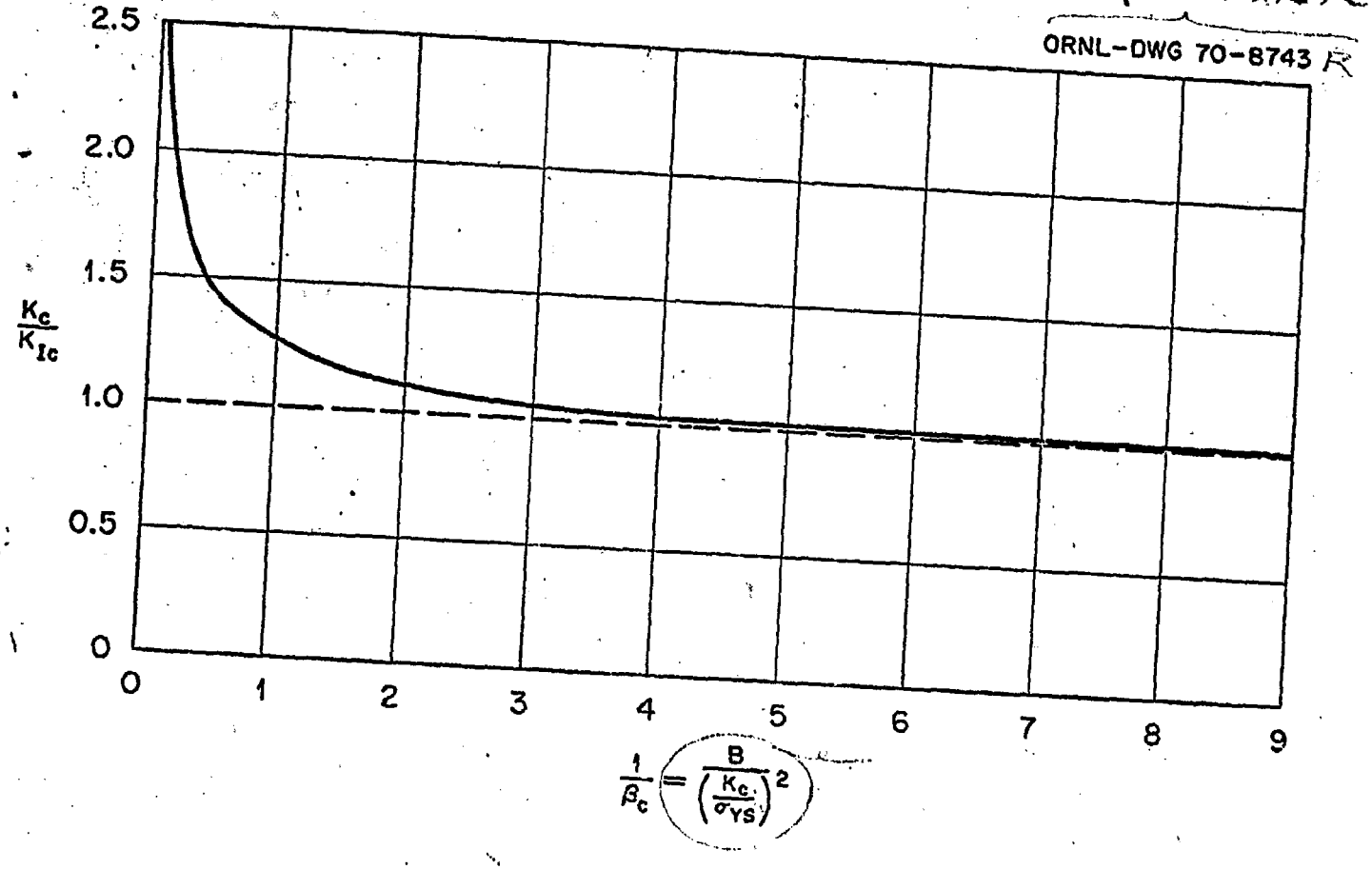

Fig. 19

TRANSVERSE RESTRAINT EFFECTS

$$\left(\frac{K_c}{K_{Ic}}\right)^2 = 1 + 1.4\,\beta_{Ic}^2$$

$$\beta_{Ic} = \frac{\left(\frac{K_{Ic}}{\sigma_Y}\right)^2}{B}$$

B = THICKNESS

RE-ARRANGING:

$$\frac{1}{\beta_c} = \frac{1.182}{\left(\frac{K_c}{K_{Ic}}\right)^2\left[\left(\frac{K_c}{K_{Ic}}\right)^2 - 1\right]^{1/2}}$$

$$\beta_c = \frac{\left(\frac{K_c}{\sigma_Y}\right)^2}{B}$$

d) HYPOTHESIS OF A RESTRAINT DISTANCE

THROUGH CRACK

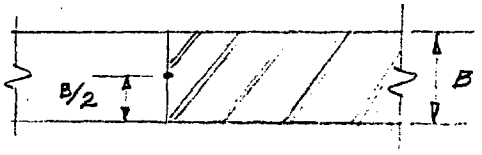

$$d_r = \frac{B}{2}$$

$$B = 2d_r$$

$$\beta_c = \frac{\left(\frac{K_c}{\sigma_Y}\right)^2}{2d_r}$$

PART-THROUGH CRACK

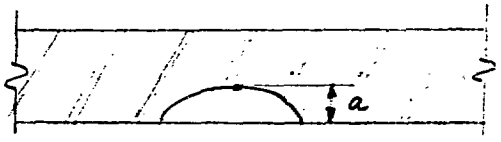

$$d_r = a$$

(EXPERIMENTS INDICATE OK FOR A TENSILE SPECIMEN, BUT NOT FOR THE CYLINDRICAL REGION OF A PRESSURE VESSEL) →

$$\beta_c = \frac{\left(\frac{K_c}{\sigma_Y}\right)^2}{2a}$$

FACTORS INFLUENCING THE EFFECTIVE TOUGHNESS:

1. DIMENSIONS (CRACK SIZE &/OR THICKNESS)
2. PLANE STRAIN TOUGHNESS
3. YIELD STRESS

LINEAR ELASTIC FRACTURE MECHANICS, EXPRESSED IN TERMS OF STRAIN

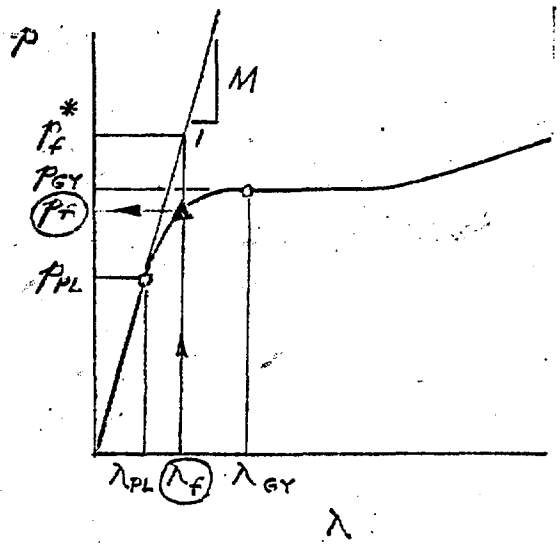

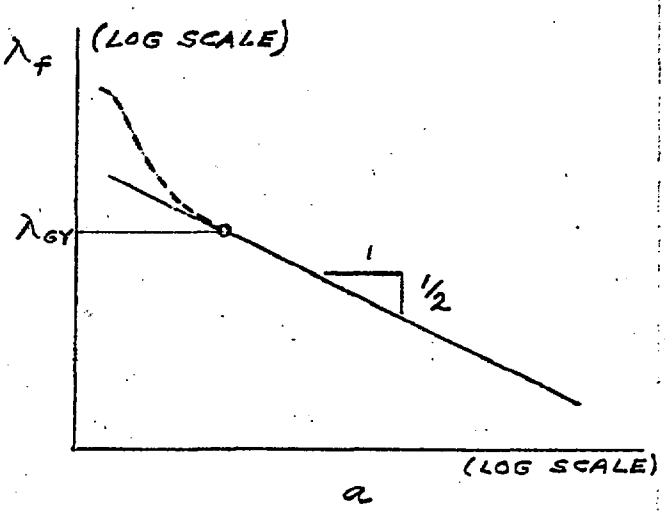

FOR ELASTIC CONDITIONS,

$$K_{Ic} = C p_f \sqrt{\pi a}$$

$$p_f = \frac{K_{Ic}}{C\sqrt{\pi a}}$$

BETWEEN p_{PL} AND p_{GY}

$$p_f^* = \frac{K_{Ic}}{C\sqrt{\pi a}}$$

$$\lambda_f = \frac{p_f^*}{M}$$ ← FAILURE STRAIN ESTIMATED AS A TOTALLY ELASTIC STRAIN

DETERMINE THE ACTUAL p_f AS THE PRESSURE CORRESPONDING TO THE STRAIN λ_f, ACCORDING TO THE PRESSURE - STRAIN DIAGRAM.

PROPOSED METHODS FOR ELASTIC - PLASTIC FRACTURE ANALYSIS (CONT'D)

4. THE TANGENT MODULUS METHOD

a) DERIVATION OF THE METHOD

$$K_\sigma K_\epsilon = K_t^2 \qquad \text{NEUBER'S EQUATION}$$

$$K_\sigma = \frac{d\sigma}{dS} \; ; \qquad K_\epsilon = \frac{d\epsilon}{d\lambda} \; ; \qquad K_t = 2C\sqrt{\frac{a}{\rho}}$$

$$\frac{d\sigma}{dS} \cdot \frac{d\epsilon}{d\lambda} = \left(2C\sqrt{\frac{a}{\rho}}\right)^2$$

$d\sigma = E_n \, d\epsilon$, $E_n = E_s$, THE STRAIN HARDENING TANGENT MODULUS

$dS = E_g \, d\lambda$, E_g IS THE TANGENT MODULUS CORRESPONDING TO THE GROSS STRAIN, λ

$$\frac{E_n}{E_g}\left(\frac{d\epsilon}{d\lambda}\right)^2 = \left(2C\sqrt{\frac{a}{\rho}}\right)^2$$

$$\boxed{d\epsilon\sqrt{\rho} = 2C\sqrt{a}\sqrt{\frac{E_g}{E_n}}\, d\lambda}$$

$$\boxed{\epsilon_f\sqrt{\rho} = \frac{2}{\sqrt{\pi}}\sqrt{\frac{E}{E_s}}\left(\frac{K_c}{S_Y}\right)\lambda_Y}$$

FOR ρ = CONST.,

$$\int d\epsilon\sqrt{\rho} = \epsilon\sqrt{\rho}.$$

FOR $d\epsilon = \frac{d\rho}{\rho}$ & $\delta = 2\rho$,

$$\int d\epsilon\sqrt{\rho} = \sqrt{2\delta}.$$

b) APPLICATIONS

MODEL VESSELS → INTERMEDIATE TENSILE SPECIMENS

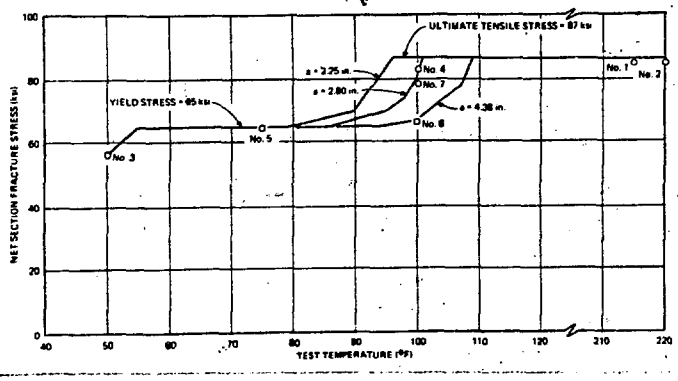

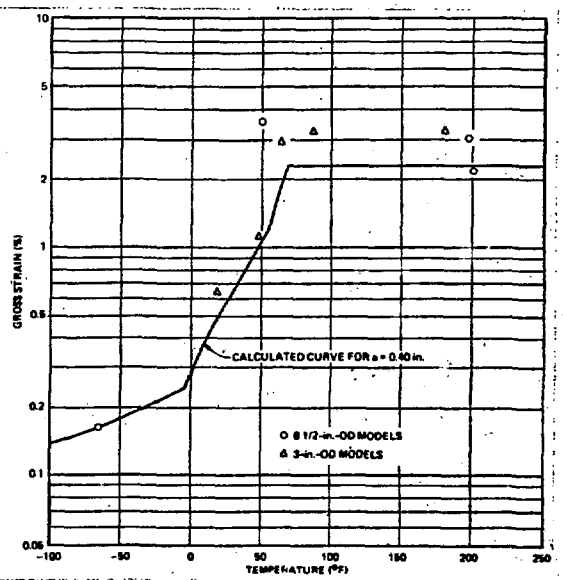

TANGENT MODULUS EQUATIONS FOR THE CASE OF BENDING

1. THE EFFECTIVE TANGENT MODULUS, E_g, IS DEFINED AS THE AVERAGE TANGENT MODULUS ACROSS THE SECTION CONTAINING THE CRACK.

2. FOR THE CASE OF A LINEAR STRAIN GRADIENT INDUCED BY BENDING, THE EFFECTIVE TANGENT MODULUS IS FOUND TO BE THE SECANT MODULUS AT THE SURFACE.

3. THE RESULTING EQUATIONS, FOR A TRILINEARIZED STRESS-STRAIN CURVE AND AN APPLIED STRAIN IN THE STRAIN HARDENING RANGE, ARE:

a) FOR THE ELASTIC RANGE,

$$\Delta\epsilon\sqrt{\rho} = 2C\sqrt{a}\sqrt{E/E_s}\,\lambda_Y \quad ;$$

b) FOR THE TRANSITION RANGE,

$$\Delta\epsilon\sqrt{\rho} = 4C\sqrt{a}\sqrt{E/E_s}\left(\sqrt{\lambda_s\lambda_Y} - \lambda_Y\right) \quad ;$$

c) FOR THE STRAIN HARDENING RANGE,

$$\Delta\epsilon\sqrt{\rho} = 2C\sqrt{a}\left\{\sqrt{\lambda_f(\lambda_f+\lambda_d)} - \sqrt{\lambda_s(\lambda_s+\lambda_d)} + \lambda_d \ln\left(\frac{\sqrt{\lambda_f}+\sqrt{\lambda_f+\lambda_d}}{\sqrt{\lambda_s}+\sqrt{\lambda_s+\lambda_d}}\right)\right\} \quad ,$$

WHERE $\lambda_d = \dfrac{S_Y}{E_s} - \lambda_s$.

4. TRILINEARIZED $S-\lambda$ CURVE →